


Article

# Preparation and Application of Organic-Inorganic Nanocomposite Materials in Stretched Organic Thin Film Transistors

Yang-Yen Yu <sup>1,2,\*</sup>  and Cheng-Huai Yang <sup>1</sup>

<sup>1</sup> Department of Materials Engineering, Ming Chi University of Technology, New Taipei City 243, Taiwan; harry830308@gmail.com

<sup>2</sup> Department of Chemical and Materials Engineering, Chang Gung University, Taoyuan City 33302, Taiwan

\* Correspondence: yyyu@mail.mcut.edu.tw

Received: 15 March 2020; Accepted: 2 May 2020; Published: 5 May 2020



**Abstract:** High-transparency soluble polyimide with COOH and fluorine functional groups and TiO<sub>2</sub>-SiO<sub>2</sub> composite inorganic nanoparticles with high dielectric constants were synthesized in this study. The polyimide and inorganic composite nanoparticles were further applied in the preparation of organic-inorganic hybrid high dielectric materials as the gate dielectric for a stretchable transistor. The optimal ratio of organic and inorganic components in the hybrid films was investigated. In addition, Jeffamine D2000 and polyurethane were added to the gate dielectric to improve the tensile properties of the organic thin film transistor (OTFT) device. PffBT4T-2OD was used as the semiconductor layer material and indium gallium liquid alloy as the upper electrode. Electrical property analysis demonstrated that the mobility could reach 0.242 cm<sup>2</sup>·V<sup>-1</sup>·s<sup>-1</sup> at an inorganic content of 30 wt.%, and the switching current ratio was 9.04 × 10<sup>3</sup>. After Jeffamine D2000 and polyurethane additives were added, the mobility and switching current could be increased to 0.817 cm<sup>2</sup>·V<sup>-1</sup>·s<sup>-1</sup> and 4.27 × 10<sup>5</sup> for Jeffamine D2000 and 0.562 cm<sup>2</sup>·V<sup>-1</sup>·s<sup>-1</sup> and 2.04 × 10<sup>5</sup> for polyurethane, respectively. Additives also improved the respective mechanical properties. The stretching test indicated that the addition of polyurethane allowed the OTFT device to be stretched to 50%, and the electrical properties could be maintained after stretching 150 cycles.

**Keywords:** soluble polyimide; polyurethane; Jeffamine; organic-inorganic hybrid film; Stretchable transistor

## 1. Introduction

Stretchable electronic components have attracted much research interest due to their considerable potential in biomedical instruments, smart skins, displays, and battery devices [1–3]. From 2010 to 2020, thin film transistors have been made predominantly from inorganic materials. The main reason for this is that the carrier mobility values of organic materials are too low compared with those of inorganic materials [4]. Because the performance of an organic thin film transistor (OTFT) [5,6] has not been able to reach the same performance of inorganic transistor, researchers have continued to study the use of various semiconductor materials [7–11] to improve their carrier mobility. In addition, the plastic soft board-based OTFTs can also be used on flexible substrates [12–15]. The rise of plastic substrates [16–18] has necessitated some flexural quality measurements and novel processing methods, such as stretching and coating, to increase the flexibility and mobility of components [19,20]. A roll-to-roll process that can be fabricated on a flexible substrate in a low-temperature environment could support future commercial development [21].

Hybrid materials [22–24] are organic-inorganic polymer blends that are molecularly mixed and blended through van der Waals forces, hydrogen bonds, ionic bonds, or covalent bonds, thus overcoming

the phase separation that can usually be observed in traditional materials. These hybrid materials have the advantages of organic and inorganic materials, providing excellent material properties, including thermal, mechanical, optical, and electrical properties. To achieve a good nanoscale dispersion of organic-inorganic materials, the sol-gel method is the most commonly used method because it is flexible and materials prepared with the sol-gel method have high thermal stability and optical transparency.

This study used spin coating to replace the traditional vaporization for the fabrication of thin film transistors. Polyimide [25–27] was used for the preparation of OTFT due to its good thermal stability, chemical resistance, and mechanical properties. As practical applications continue to advance, the requirements for thermal and mechanical properties are becoming more and more demanding, so inorganic materials are often used to enhance the relevant properties. The most common inorganic materials are  $\text{SiO}_2$  and  $\text{TiO}_2$ , which can be prepared using tetraethoxysilane (TEOS) and titanium butoxide, respectively. The use of inorganic composite material  $\text{TiO}_2$ - $\text{SiO}_2$  has also been featured in the literature [28,29]. Such an organic-inorganic hybrid film [30] was applied in OTFT as a dielectric film. The donor material, PffBT4T-2OD [31], was also used to replace the traditional pentacene [32] as a semiconductor layer in organic photovoltaic devices. However, PffBT4T-2OD has not been applied to OTFTs in other research.

Electronic products increasingly require the properties of flexibility and stretchability [33–37]. Therefore, some suitable polymers have been added to these advanced electronic products [38,39], such as Jeffamine D2000 [40] and polyurethane [41]. Another approach to enhance flexibility and stretchability is to connect the sidechain of the semiconductor layer material with an elastic polymer, such as poly(butyl acrylate)(PBA) or 2,6-pyridine dicarboxamide (PDCA). After this modification, the researchers expected that the device could retain its original performance after being subjected to stretching many cycles. The chemical structures of the polyimide- $\text{TiO}_2$ - $\text{SiO}_2$ , Jeffamine D2000, and polyurethane as well as the structural diagrams for the OTFT device and the experimental stretching directions are shown in Figure 1. Tensile properties depend on the ratio of  $\text{TiO}_2$ - $\text{SiO}_2$  and whether Jeffamine D2000 or polyurethane is added. The addition ratio of  $\text{TiO}_2$ - $\text{SiO}_2$  ranges from A0–A40 in the order of 0 wt.% to 40 wt.%, B0–B40 when Jeffamine D2000 is added, and C0–C40 when polyurethane is added.

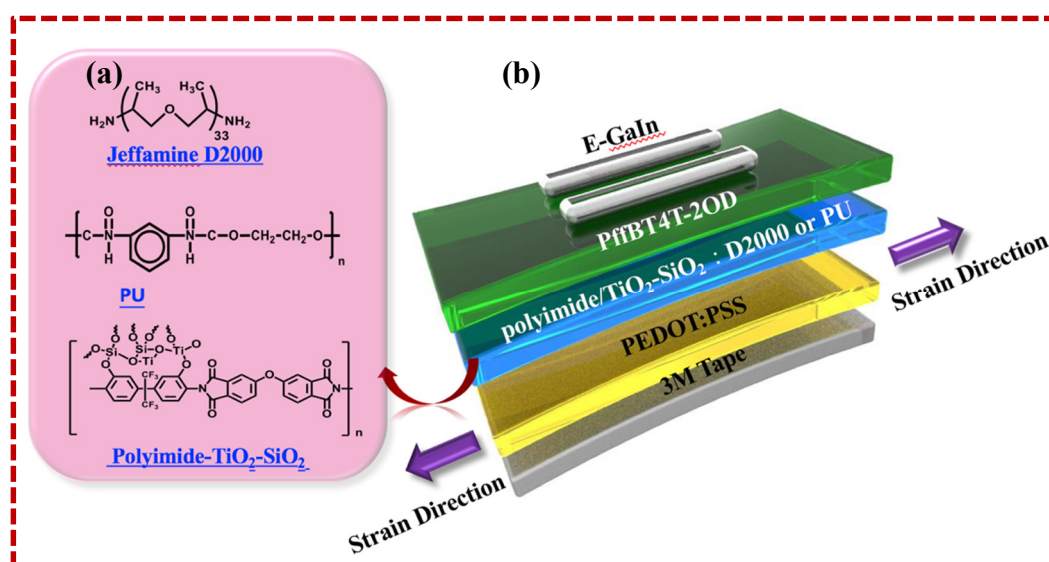


**Figure 1.** (a) Chemical structures of polyimide- $\text{TiO}_2$ - $\text{SiO}_2$ , Jeffamine D2000, and PU. (b) Device structure with illustration of each layer and strain direction in an organic thin film transistor.

## 2. Experimental Section

In this study, a stretchable OTFT was fabricated using Elastomer Tape 3M tape as the stretchable substrate and poly(3,4-ethylenedioxythiophene) polystyrene sulfonate (PEDOT:PSS, Sigma Aldrich, Darmstadt, Germany) as the lower electrode.  $\text{TiO}_2\text{-SiO}_2$  inorganic nanoparticles and a soluble polyimide with COOH and a fluorine atom functional group were used to prepare the dielectric layer. The COOH on polyimide could be hydrolyzed and condensed with  $\text{TiO}_2\text{-SiO}_2$  to form a dense network structure, and the size of the CF group in PI molecule is quite big, which can cause an increase of free volume and a reduction of the interaction between the molecular chains, so as to increase the solubility and transparency for the prepared polyimide- $\text{TiO}_2\text{-SiO}_2$  hybrid films. The film was used as an OTFT gate dielectric. In addition, soluble polyimide overcame the problem of the high temperature dehydration cyclization of thermal polymerization and was applicable to a stretchable OTFT device. In addition, Jeffamine D2000 and polyurethane could be used as additives to increase the tensile properties without the original electrical properties being affected.

### 2.1. Preparation of Dielectric Gate Dielectric

Briefly, the 4,4-oxydiphthalic anhydride (97%, Sigma Aldrich, Darmstadt, Germany) and the 2,2-bis(3-amino-4-hydroxyphenyl) hexafluoropropane (98%, Matrix Scientific, Columbia, SC, USA) in a three-necked flask were dissolved in the *n*-methyl-2-pyrrolidone (NMP, 99.9%, TEDIA, USA) with 1:1 molar ratio and mixed uniformly. After the further addition of isoquinoline (95%, Tokyo Chemical Industry) in a nitrogen atmosphere for 5 h, a yellow-brown solution was obtained, which was poly(amic acid) (PAA). The PAA was placed in an oil bath at 150 °C for 18 h. The polyimide solution obtained was placed in a water: methanol (98%, Mallinckrodt Baker, Phillipsburg, KS, USA) (1:3) mixed solvent to produce the precipitate. The filtrated precipitate was placed in a vacuum oven and dried at 60 °C for 2 days to obtain a soluble polyimide powder containing COOH and a fluorine functional group. Tetraethyl orthosilicate (TEOS, Sigma Aldrich, Darmstadt, Germany) was dissolved in ethanol (99.5%, Acros Organics, NJ, USA) added to an aqueous solution of nitric acid, and stirred for 30 min. Simultaneously, titanium(IV) butoxide ( $\text{Ti}(\text{O}i\text{Bu})_4$ , Sigma Aldrich, Darmstadt, Germany) was dissolved in 2-methyl-2,4-pentanediol (98%, Alfa Aesar, MA, USA) solvent, stirred for 30 min. The two aforementioned solutions were mixed and stirred for sol-gel reaction for 30 min, and the solvent was then removed with a rotary evaporator and finally placed in an oven to obtain the  $\text{TiO}_2\text{-SiO}_2$  inorganic nanoparticles. The polyimide dissolved in *N,N*-Dimethylacetamide (DMAc, 99.8%, TEDIA, USA) and the  $\text{TiO}_2\text{-SiO}_2$  nanoparticles dispersed in butanol solvent were mixed and stirred for 30 min to prepare three series of hybrid materials, namely polyimide- $\text{TiO}_2\text{-SiO}_2$ , polyimide- $\text{TiO}_2\text{-SiO}_2\text{:D2000}$ , and polyimide- $\text{TiO}_2\text{-SiO}_2\text{:PU}$ . To prepare the polyimide- $\text{TiO}_2\text{-SiO}_2$  hybrid material, the different ratios of  $\text{SiO}_2\text{-TiO}_2$  (0, 10, 20, 30, and 40 wt.%) were mixed with polyimide and stirred for 1 h to obtain the PI- $\text{TiO}_2\text{-SiO}_2$  precursor solution represented by AX (X = weight percentage of  $\text{SiO}_2\text{-TiO}_2$  in hybrid material). For preparation of the polyimide- $\text{TiO}_2\text{-SiO}_2\text{:D2000}$  and polyimide- $\text{TiO}_2\text{-SiO}_2\text{:PU}$  hybrid material, the preparation procedure was the same as for polyimide- $\text{SiO}_2\text{-TiO}_2$ . The only difference was that the polymer (Jeffamine D2000, Alfa Aesar, Massachusetts, USA) or polyurethane, (Sigma Aldrich, Darmstadt, Germany) was dropped gradually into the polyimide solution before the mixing with  $\text{TiO}_2\text{-SiO}_2$  inorganic nanoparticles. The polyimide- $\text{TiO}_2\text{-SiO}_2\text{:D2000}$  and polyimide- $\text{TiO}_2\text{-SiO}_2\text{:PU}$  hybrid materials were represented by BX and CX, respectively, where X was the weight proportion of  $\text{SiO}_2\text{-TiO}_2$  in the hybrid material.

### 2.2. OTFT Device Preparation

First, the elastomer tape was attached to the glass and subjected to plasma treatment for 3 min to clean the tape surface. PEDOT:PSS was then spin coated on the elastomer tape and annealed at 100 °C for 30 min. The solution of polyimide- $\text{SiO}_2\text{-TiO}_2$  (or polyimide- $\text{SiO}_2\text{-TiO}_2\text{:Jeffamine D2000}$  or polyimide- $\text{TiO}_2\text{-SiO}_2\text{:polyurethane}$ ) was spin coated onto PEDOT:PSS elastomer tape at 2000 rpm/20 s.

The coated wafer was placed on a hot plate and thermally polymerized through stepwise heating. The baking process was performed at 60, 80, and 100 °C for 10 min and then, finally, at a temperature of 120 °C for 10 min. Three series of hybrid dielectric films, namely AX, BX, and CX, were obtained. The poly[(5,6-difluoro-2,1,3-benzothiadiazol-4,7-diyl)-alt-(3,3''-di(2-octyldodecyl)-2,2',5',2'',5'',2'''-quaterthiophen-5,5''-diyl)] (PffBT4T-2OD, Sigma Aldrich) as the active layer was then spin coated onto the dielectric layer on a hot plate and heated at 90 °C for 5 min as an annealing process. The upper electrode (source and drain) EGaIn (99.99%, Alfa Aesar, MA, USA) was dropped onto the lower electrode and the PffBT4T-2OD surface, respectively, to fabricate the OTFT device. The device structure is shown in Figure 1.

### 2.3. Characterization

The thermal properties of the prepared hybrids were assessed using a thermogravimetric analysis (TGA, TA Instruments, Q50) and differential scanning calorimeter analysis (DSC, TA Instruments, Q20/RSC90) at heating rates of 20 °C and 10 °C/min, respectively. The transmittances of the hybrid films coated on the quartz substrates were collected using an ultraviolet-visible spectrum (UV-Vis, Jasco, V-650). The morphologies of the thin films were observed with a high-resolution transmission electron microscope (HR-TEM, JEOL, JEM-2100), a scanning electron microscope (SEM, Hitachi, H-2400), and an atomic force microscope (AFM, Veeco, DI 3100). The thicknesses of the hybrid thin films were analyzed with a microfigure measuring instrument (Surface Profiler,  $\alpha$ -step, ET-4000, Kosaka Laboratory Ltd.). For the metal-insulator-metal (MIM) structure analysis, 0.6-mm diameter Al electrodes were deposited directly onto the gate dielectric films through shadow masking. MIM direct current measurements and OTFT measurements were performed in ambient conditions using a probe station interface with an Agilent E4980A precision LCR meter (10 kHz to 1 MHz) and an Agilent B1500A semiconductor device parameter analyzer.

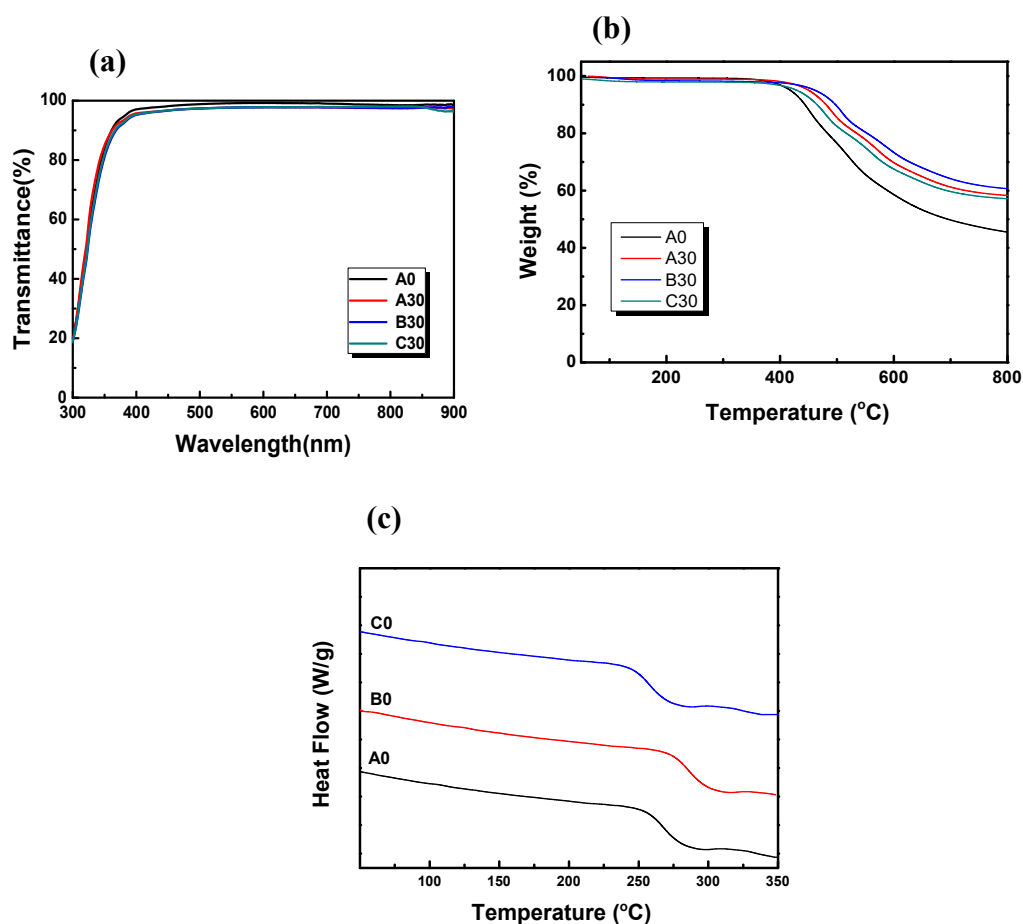
## 3. Results and Discussion

Figure 1 shows the chemical structures of the polyimide-TiO<sub>2</sub>-SiO<sub>2</sub> composite dielectric material, Jeffamine D2000, and polyurethane additives and the schematic for the OTFT device structure and the tensile direction. The OTFT devices exhibit tensile properties that depend on the addition ratio of TiO<sub>2</sub>-SiO<sub>2</sub> inorganic nanoparticles and the presence or absence of Jeffamine D2000 or polyurethane additives. The addition ratio of TiO<sub>2</sub>-SiO<sub>2</sub> inorganic nanoparticles ranges from 0 wt.% to 40 wt.%; the cases with those ratio values are denoted by A0–A40, B0–B40, and C0–C40, respectively, indicate the addition of Jeffamine D2000 and polyurethane additives in the order of 0 wt.% to 40 wt.%.

### 3.1. Analysis of Optical and Thermal Properties

All of the prepared hybrid films have optical transmittances greater than 90% with the film thickness about 200 nm. Figure 2a shows the UV-vis spectra of the optical transmittance of A0, A30, B30, and C30 hybrid thin films in the visible light region of 400–700 nm, the optical transmittance is greater than 90%. This result shows that the composite dielectric film has good transparency (as listed in Table 1). Supplementary Figure S1 shows the TEM image of inorganic TiO<sub>2</sub>-SiO<sub>2</sub> nanoparticles. It shows that the size of the particles of the as-prepared TiO<sub>2</sub>-SiO<sub>2</sub> is about 30–40 nm with a spherical morphology. When the particle size is less than 50 nm, light scattering can be negligible [42]. Moreover, Supplementary Figure S2 shows the optical transmittance of A0, A30, B30, and C30 films as the dielectric layer of OTFTs device in the visible light region of 400–700 nm. This indicates that the optical transmittances of all samples are greater than 75%. The thermal properties of the prepared polyimide-TiO<sub>2</sub>-SiO<sub>2</sub> composite dielectric films were analyzed by thermogravimetric analysis (TGA). Figure 2b shows the TGA curves undertaken in a nitrogen atmosphere. It reveals that the decomposition temperature ( $T_d$ ) of A0, A30, B30, and C30 hybrid thin films are 418, 450, 461, and 443 °C, respectively. The relative parameters for thermal properties are listed in Table 1. This indicates that the thermal decomposition temperature increases with the content of TiO<sub>2</sub>-SiO<sub>2</sub> nanoparticles due to the formation

of chemical bonding between polyimide and  $\text{TiO}_2\text{-SiO}_2$ , which can restrict the polyimide chain reaction, and the  $T_d$  and thermal stability for the hybrid films thus increases as  $\text{TiO}_2\text{-SiO}_2$  content increases [22]. In addition, the addition of Jeffamine D2000 and polyurethane also increase the  $T_d$  from 426 °C to 477 °C for B0–B40 and 405 °C to 454 °C for C0–C40. The increase in  $T_d$  for B0–B40 is due to the hydrogen bonding between the N atom in the Jeffamine D2000 and the composite dielectric material. However, the polyurethane is a softer polymer, so the  $T_d$  of B0–B40 is expected to be lower than that for the other two series of hybrid films. However, the  $T_d$  for all of hybrid films nonetheless exceed 400 °C, indicating good thermal stability. In addition, none of the hybrid films exhibit weight loss at temperatures lower than 300 °C, and the residual quantity of A0–A40 increased with increasing quantities of  $\text{TiO}_2\text{-SiO}_2$  added when the temperature increased to 900 °C. At 900 °C most of the polyimide has completely decomposed, and the remaining residual quantity is an inorganic oxide forming a cross-linked stable network. This result demonstrates that inorganic  $\text{TiO}_2\text{-SiO}_2$  nanoparticles have been successfully incorporated into organic materials. Figure 2c shows the differential scanning calorimeter analysis (DSC) measured in a nitrogen atmosphere. It reveals that the glass transition temperatures ( $T_g$ ) of A0 (PI), B0 (PI:D2000), and C0 (PI:PU) are 266 °C, 286 °C, and 270 °C, respectively. In addition, no  $T_g$  point of all samples can be observed in Figure 2c in the temperature range of 25–350 °C, showing the  $T_g$  of all hybrid materials (PI/ $\text{TiO}_2\text{-SiO}_2$ ) prepared in this study exceeds 350 °C (as listed in Table 1). It is known that the inorganic  $\text{TiO}_2\text{-SiO}_2$  nanoparticles can be uniformly distributed in the polyimide matrix, and form a crosslinking structure between the polyimide and nanoparticles, which restricts the chain motion and strengthens the polyimide strength, thereby causing an increase in  $T_g$  and  $T_d$ . The results of thermal analysis suggest that all of the hybrid films prepared in this study exhibit good heat resistance and no phase separation between the polyimide and  $\text{TiO}_2\text{-SiO}_2$  nanoparticles [43].



**Figure 2.** (a) UV-vis spectra of the optical transmittance, (b) TGA curves, and (c) DSC curves of hybrid thin films.

**Table 1.** Summary of properties of the prepared dielectric hybrid film.

No.	H (nm) <sup>a</sup>	Ra (nm) <sup>b</sup>	Ra/h (%)	T <sub>d</sub> (°C)	T <sub>g</sub> (°C)	T (%)
A0	215	0.44	0.20	418	266	
A10	200	0.56	0.28	427	-	
A20	215	0.61	0.28	431	-	>90%
A30	220	0.65	0.29	450	-	
A40	210	0.75	0.35	461	-	
B0	200	0.31	0.15	426	286	
B10	210	0.35	0.17	431	-	
B20	220	0.41	0.19	440	-	>90%
B30	215	0.57	0.27	461	-	
B40	215	0.64	0.29	477	-	
C0	220	0.43	0.19	405	270	
C10	210	0.49	0.23	419	-	
C20	220	0.53	0.24	432	-	>90%
C30	215	0.60	0.28	443	-	
C40	210	0.69	0.33	454	-	

<sup>a</sup> Thickness of the prepared thin film. <sup>b</sup> Ra is the average roughness of the prepared thin films, respectively.

### 3.2. Analysis of Stretching Properties

Figure 3 shows the optical microscopy images of (a) A0, B0, and C0 and of (b) A30, B30, and C30 thin films subject to various strain levels. Figure 3a shows that bare polyimide film generates cracks when subjected to a stretching ratio of 30%, and numerous cracks and wrinkles are produced when the stretching ratio reaches 50%. The B0 film exhibits only wrinkles under the stretching ratio of 30%, but numerous cracks are also present as the stretching ratio increases to 50%. Compared with the result for A0, the addition of Jeffamine D2000 (B0) is seen to improve the film's stretchability. For the C0, the film shows no cracks or wrinkles subject to stretching ratios of 30% and 50%. The results reveal that the addition of polyurethane is more effective than the addition of Jeffamine D2000 for improving the tensile properties of the thin films in the absence of inorganic particles in the polyimide matrix. Moreover, the effect of nanoparticles TiO<sub>2</sub>-SiO<sub>2</sub> on the tensile properties is seen in Figure 3b. Adding TiO<sub>2</sub>-SiO<sub>2</sub> is seen to cause the tensile properties of the A30 films to decrease obviously because more cracks are observed for a stretching ratio of 30%. For the case of B30 films, wrinkles continue to be generated at a stretching ratio of 30%, but no cracks are observed. The C30 films' stretchability is optimal at the stretching ratios of 30% and 50%. No cracks or wrinkles are observed on the C30 films. Therefore, from the optical microscopy diagram of these dielectric hybrid films, the addition of Jeffamine D2000 and polyurethane polymers is seen to increase the film stretchability and the addition of polyurethane produces tensile properties superior to those obtained from the addition of Jeffamine D2000.



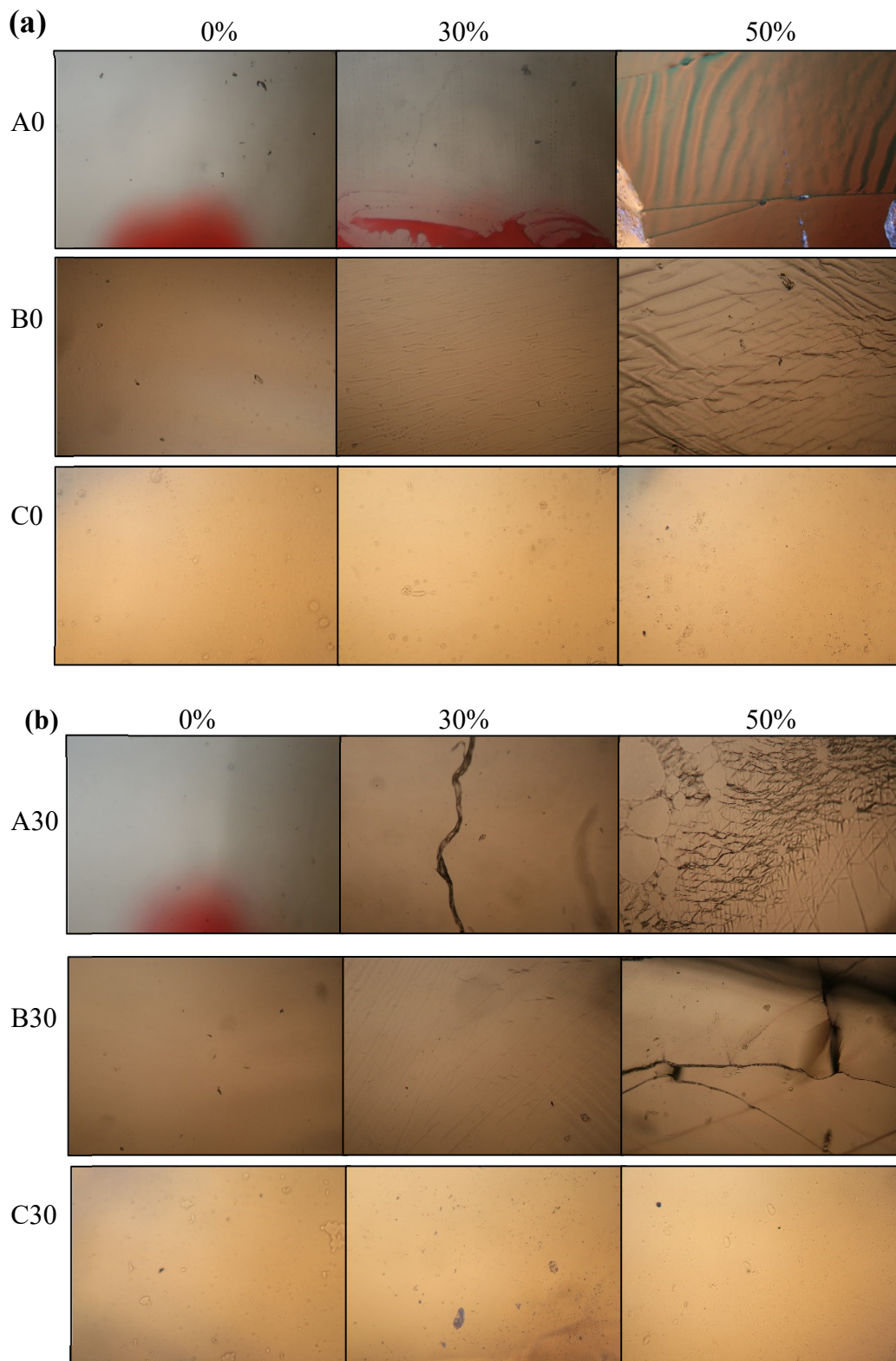


**Figure 3.** Optical microscopy images of (a) A0, B0, and C0 and of (b) A30, B30, and C30 thin films subject to various strain levels.

### 3.3. Analysis of Surface Morphology and Surface Energy

The surface flatness of the hybrid dielectric films was measured using an atomic force microscope (AFM). The AFM result demonstrates that the surface roughness ( $R_a$ ) of the three series of A0–A40, B0–B40, and C0–C40 are 0.44–0.75, 0.31–0.64, and 0.43–0.69 nm, respectively.  $R_a$  increases with the increase in  $\text{TiO}_2$ - $\text{SiO}_2$  content. However, all hybrid dielectric films were produced without pinholes, and the surface flatness (the ratio of  $R_a$  to film thickness,  $R_a/h$ ) for all hybrid films was less than 0.35% (Table 1), indicating that all prepared hybrid dielectric films in this study had a good surface flatness. In the previous studies, it has been confirmed that, when the ratio of surface roughness to thickness is less than 0.5%, the material has a good flatness. The prepared dielectric thin film in this study has a better surface flatness than those of studies in literature [39,42,43]. According to the aforementioned results, the three series of hybrid dielectric films have good light transmission, thermal stability, and surface flatness, and no phase separation was observed. Therefore, the prepared hybrid dielectric films can be effectively applied as the gate dielectric materials for the OTFT application.

Typically, thin films show a light scattering behavior due to the surface roughness. An innovative hybrid thin film with a lower-than-usual surface roughness can reduce the light loss on the waveguide surface. This result also confirms the potential for the use of polyimide- $\text{TiO}_2$ - $\text{SiO}_2$  hybrid material in OTFT as the dielectric film. The surface flatness of the dielectric layer greatly influences the characteristics of the OTFT. When the dielectric layer has a low surface roughness, it effectively reduces the leakage current of OTFT and promotes the order growth of crystals in the active layer. Figure 4 shows the AFM images of the semiconductor layer (BffBT4T-2OD) coated on the various dielectric composite films, namely A0, B0, C0, A30, B30, and C30. This indicates that island-like aggregation was produced from the BffBT4T-2OD on the semiconductor layer (A30) after the addition of the inorganic nanoparticles, and the degree of aggregation became more obvious after the addition of the Jeffamine D2000 (B30) and polyurethane (C30). These dense aggregates of BffBT4T-2OD can help to increase the tensile properties of these composite films and the stretchability of OTFT [41]. BffBT4T-2OD is hydrophobic in nature, and we observed B30 to have lower surface energy ( $42.07 \text{ mJ}\cdot\text{m}^{-2}$ ) than A30 and C30 did, which enables the growth of BffBT4T-2OD. As the adding ratio of the  $\text{TiO}_2$ - $\text{SiO}_2$  nanoparticles increases, the size of BffBT4T-2OD crystal grains in the semiconductor layer also increases, resulting in better characteristics for the OTFT. This may be related to the affinity of the dielectric surface for BffBT4T-2OD. As the  $\text{TiO}_2$ - $\text{SiO}_2$  content increases from 0% (A0) to 30 wt.% (A30), the surface energy of the dielectric layer decreases, which causes the grain size of BffBT4T-2OD in semiconductor layer to increase. The well-connected domain of the A30 provides an efficient channel for charge transport and increases the charge carrier density at the interface between dielectric and semiconductor, which can prevent the charge defects from occurring at the interface and improve the performance of the OTFTs [38–40].

The contact angles of the gate dielectric films were measured using deionized water and diiodomethane as the test drops, respectively, due to their different polarities. The surface energies of the polyimide- $\text{TiO}_2$ - $\text{SiO}_2$  hybrid films could then be calculated from the values of the contact angles obtained from water and diiodomethane drops, respectively. The results are listed in Table 2. If the surface of a hybrid film has a small water contact angle, this indicates that the surface is hydrophilic and has a large surface energy. Conversely, a large water contact angle indicates that the surface is hydrophobic and has a low surface energy. As shown in Table 2, whether water or diiodomethane is used as the test drop, the contact angles for the hybrid films (A, B, and C) increase first and then decrease with the addition of inorganic particles. For A0–A40 hybrid films, the water contact angles increase from 79.78 for A0 to 83.99 for A30 and then decrease to 78.30 for A40.



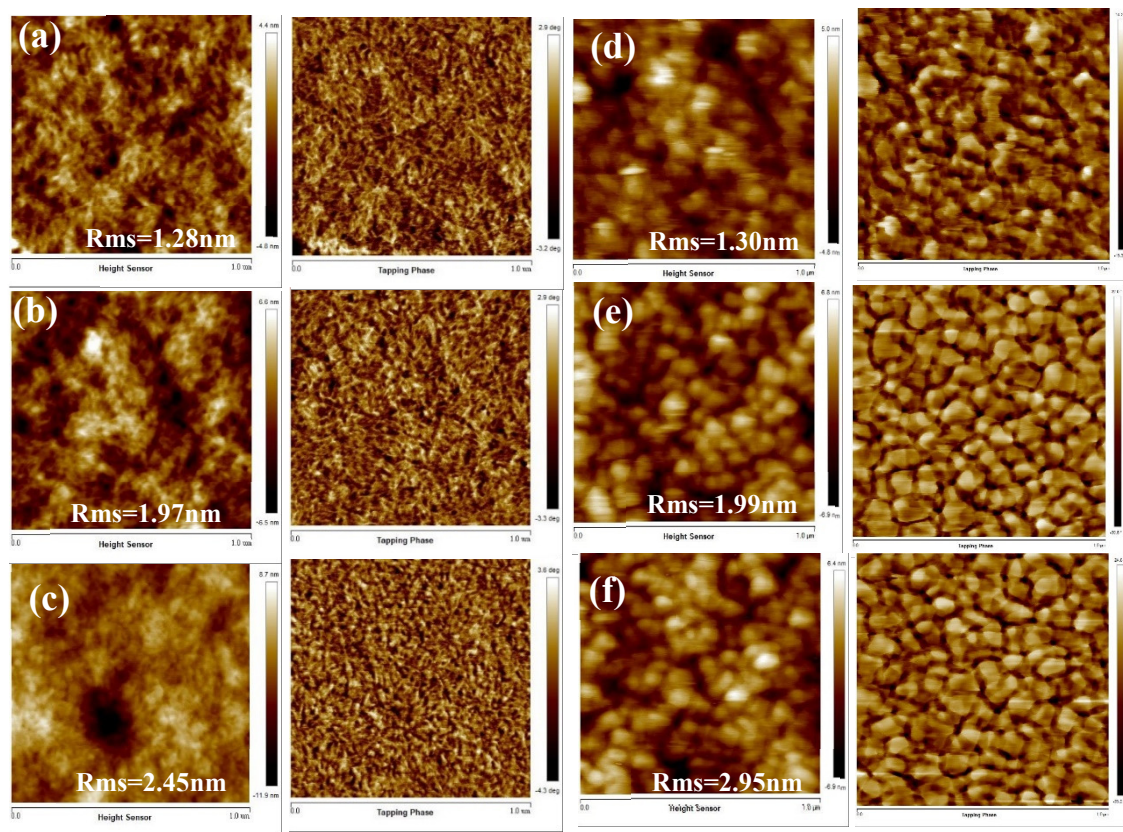


**Figure 4.** Tapping-mode AFM ( $1 \times 1 \mu\text{m}$ ) images (left: topographic images, right: phase images) of blend films deposited with various  $\text{TiO}_2\text{-SiO}_2$  ratios and addition of Jeffamine D2000 or polyurethane; (a) A0, (b) B0, (c) C0, (d) A30, (e) B30, and (f) C30.

**Table 2.** Summary of dielectric constant and surface energy for various hybrid dielectric films.

No.	Dielectric Constant [-]				Water Contact Angle [°]	Diiodomethane Contact Angle [°]	Surface Energy [ $\text{mJ}\cdot\text{m}^{-2}$ ]
	1 kHz	10 kHz	100 kHz	1 MHz			
A0	4.53	4.49	4.43	4.10	79.78	35.39	51.02
A10	5.78	5.20	4.86	4.27	80.26	42.65	47.66
A20	6.93	6.30	6.11	5.02	80.76	43.09	45.73
A30	7.24	7.08	6.75	6.35	83.99	50.53	44.17
A40	9.51	8.88	7.47	6.53	78.30	29.23	52.33
B0	4.47	4.44	4.41	4.07	78.46	39.10	48.74
B10	5.57	5.11	4.72	4.03	80.44	45.49	45.97
B20	6.03	6.02	5.98	5.00	81.17	51.38	44.68
B30	7.14	7.01	6.72	5.98	84.91	51.83	42.07
B40	8.58	7.96	7.20	6.31	76.12	37.04	51.37
C0	4.22	4.10	4.01	3.98	77.38	39.24	49.47
C10	5.44	5.07	4.69	4.00	78.60	46.55	47.20
C20	5.99	5.79	5.69	5.12	78.80	51.27	44.70
C30	6.91	6.83	6.59	5.45	82.00	51.38	43.34
C40	7.87	7.78	7.01	6.29	74.49	38.22	51.02

The increase in water contact angle is mainly due to the change in surface roughness of hybrid films. In addition, the  $\text{PI/SiO}_2\text{-TiO}_2$  hybrid films in this study have a polarizable and weakly hydrophobic surface, resulting in this dielectric layer having a low surface energy. This is a very important property for wetting of the latter deposited organic semiconductor layer, and can improve the performance of the device [44]. Therefore, when 30 wt.% of  $\text{TiO}_2\text{-SiO}_2$  was added, the surface energy of the hybrid film was lowered from  $51.02 \text{ mJ}\cdot\text{m}^{-2}$  (A0) to  $44.17 \text{ mJ}\cdot\text{m}^{-2}$  (A30), indicating that the addition of high

dielectric TiO<sub>2</sub>-SiO<sub>2</sub> in a low dielectric PI matrix can change the surface roughness of the PI/TiO<sub>2</sub>-SiO<sub>2</sub> hybrid film, which in turn affects the surface energy of the hybrid film. In addition, due to the inherent hydrophobic nature of the polymer, the addition of Jeffamine D2000 and polyurethane additives can produce a highly hydrophobic surface, which further reduces the surface energy. The results show that the lowest surface energy obtained from B30 is 42.07 mJ·m<sup>-2</sup> [31]. Typically, dielectric surfaces with low surface energy can provide a venue for the growth of organic semiconductor chains.

### 3.4. Analysis of Electrical Properties

The result of volumetric capacity measurement shows that the capacitance (at 1 kHz–1 MHz) increases as the TiO<sub>2</sub>-SiO<sub>2</sub> ratio increases, and the relationship is linear. At lower frequencies, the capacitance may increase slightly due to the increased response time available for polarization. The dielectric constant (k) is evaluated using the following equation:

$$C = \frac{k\epsilon_0 A}{d} \quad (1)$$

where C is the measured capacitance,  $\epsilon_0$  is the vacuum dielectric constant, A is the area of the capacitor, and d is the thickness of the dielectric layer. As shown in Table 2, the dielectric constants obtained at 1 kHz were 4.53 for A0, 9.51 for A40, 4.47 for B0, 8.58 for B40, 4.22 for A0, and 7.87 for A40. When a higher concentration of TiO<sub>2</sub>-SiO<sub>2</sub> was used in a film's fabrication, its dielectric constant was higher. Moreover, the electrical data of OTFTs fabricated by various hybrid dielectrics are shown in Table 3. The results show that the values of mobility ( $\mu$ ) and switch current ratio (on-off current ratios,  $I_{on}/I_{off}$ ) increase with increasing the TiO<sub>2</sub>-SiO<sub>2</sub> content. Moreover, the leakage current density (LCD) measured at  $-2 \text{ MV}\cdot\text{cm}^{-1}$  also increases as the content of TiO<sub>2</sub>-SiO<sub>2</sub> nanoparticles increases. Figure S3. shows the transfer curves of OTFTs prepared by different dielectric materials, A0, A30, B30, and C30. This indicates that the mobility and  $I_{on}/I_{off}$  of the device prepared by the polyimide dielectric layer without TiO<sub>2</sub>-SiO<sub>2</sub> nanoparticles (A0) are  $0.0181 \text{ cm}^2\cdot\text{V}^{-1}\cdot\text{s}^{-1}$  and  $1.13 \times 10^3$ , respectively. When the PI/TiO<sub>2</sub>-SiO<sub>2</sub> hybrid material (A30) was used as a dielectric layer, the mobility and  $I_{on}/I_{off}$  of device increased to  $0.242 \text{ cm}^2\cdot\text{V}^{-1}\cdot\text{s}^{-1}$  and  $9.04 \times 10^3$ . When adding Jeffamine D2000 (B30) and polyurethane (C30) additives into the dielectric layer, the mobility and  $I_{on}/I_{off}$  were further increased to  $0.817 \text{ cm}^2\cdot\text{V}^{-1}\cdot\text{s}^{-1}$  and  $4.27 \times 10^5$  for B30 and  $0.562 \text{ cm}^2\cdot\text{V}^{-1}\cdot\text{s}^{-1}$  and  $2.04 \times 10^5$  for C30, respectively, which shows that the proper amount of TiO<sub>2</sub>-SiO<sub>2</sub> nanoparticles and additives can effectively improve the device performance. The larger the  $I_{on}/I_{off}$  ratio, the better the switch characteristics of OTFTs. It is known that high-k dielectric layer could cause a low operation voltage and low power consumption. The LCD value is related to the thickness of the hybrid dielectric layer and the pinholes density, because the chemical bonding between the inorganic and polyimide can make the dielectric layer structure more dense, and the high-k dielectric can improve the capacitive coupling effect between the gate and active channel layer, which can increase the driving current and reduce the operating voltage. In addition, the surface morphology of the dielectric layer affects the structure of the deposited organic semiconductor layer, which in turn affects the performance of the device. A smooth and pinhole-free surface of dielectric layer is important for the interfacial connection during the deposition of organic semiconductor layers, because a smooth interface reduces the charge scattering sites in the channel. Reducing the current leakage from the dielectric interface has a great influence on the electrical performance of the OTFTs. For high-performance OTFTs, the gate dielectric should have a low LCD and a high-k, which can provide greater surface charge accumulation and simultaneously reduce the operating voltage. It should be noted that the thickness of the dielectric layer must be carefully controlled to minimize the current leakage without greatly reducing the capacitance [44]. An increase in the LCD value means that the effect of the insulating layer is reduced. As shown in Table 3, the LCD values of all dielectric layers were less than  $10^{-8} \text{ A}\cdot\text{cm}^{-2}$ . Therefore, these hybrid dielectric layers are suitable for OTFT applications. The gate-current behavior is usually similar to the capacitor leakage current. In this work, we used a metal-insulator-metal capacitor to study the

dielectric leakage current. Moreover, as the surface energy decreases, the particle size and alignment of the semiconductor layer become denser, and the carrier mobility of the OTFT increases. Namely, more hydrophobic material increases the carrier mobility of the OTFT. Therefore, the increase in inorganic content helps to form a good organic polymer film, reducing the structural defects in the film and increasing compactness, thus improving carrier mobility. However, the device mobility decreases when the TiO<sub>2</sub>-SiO<sub>2</sub> content is more than 30 wt.%, which may be attributed to the coarser surface and the aggregation of the TiO<sub>2</sub>-SiO<sub>2</sub> particles, disturbing the formation of BffBT4T-2OD crystal structure in the semiconductor layer. Supplementary Figure S4 shows the output characteristics of the OTFTs using (a) (A0), (b) A30, (c) B30 and (d) C30 as the dielectric layer, respectively. The threshold voltages ( $V_t$ ) of OTFTs based on hybrid films are small, so only a small gate voltage is needed to turn on the gate. Surface polarization may result in smaller threshold voltages, which can lead to the filling defects of local carrier. Most of the  $V_t$  displacement is affected by three factors, which are the charge defect trapping, surface polarization, and ions. In this study, the variation of  $V_t$  displacement might be attributed to the addition of different proportions of inorganic nanoparticles at the interface between the dielectric and the semiconductor layers [45,46].

**Table 3.** The electrical data of OTFTs fabricated by various hybrid dielectrics.

No	LCD [ $\text{A}\cdot\text{cm}^{-2}$ ] (at $-2 \text{ MV}\cdot\text{cm}^{-1}$ )	$V_t$ [V]	$\mu$ [ $\text{cm}^2\cdot\text{V}^{-1}\cdot\text{s}^{-1}$ ]	$I_{\text{ON}}/I_{\text{OFF}}$ [-]
A0	$7.5 \times 10^{-10}$	-2.1	$1.81 \times 10^{-2}$	$1.13 \times 10^3$
A10	$1.5 \times 10^{-9}$	4.1	$7.01 \times 10^{-2}$	$3.24 \times 10^3$
A20	$2.7 \times 10^{-9}$	-2.3	$1.21 \times 10^{-1}$	$5.57 \times 10^3$
A30	$4.8 \times 10^{-9}$	-7.3	$2.42 \times 10^{-1}$	$9.04 \times 10^3$
A40	$7.7 \times 10^{-9}$	3.2	$1.07 \times 10^{-2}$	$1.16 \times 10^3$
B0	$6.3 \times 10^{-10}$	3.3	$5.04 \times 10^{-2}$	$1.51 \times 10^4$
B10	$8.6 \times 10^{-10}$	-1.5	$2.09 \times 10^{-1}$	$2.24 \times 10^4$
B20	$1.7 \times 10^{-9}$	3.9	$4.23 \times 10^{-1}$	$3.01 \times 10^4$
B30	$2.5 \times 10^{-9}$	-8.1	$8.17 \times 10^{-1}$	$4.27 \times 10^5$
B40	$5.8 \times 10^{-9}$	2.2	$5.51 \times 10^{-1}$	$8.50 \times 10^4$
C0	$5.9 \times 10^{-10}$	4.6	$4.81 \times 10^{-2}$	$8.13 \times 10^3$
C10	$7.7 \times 10^{-10}$	2.4	$1.89 \times 10^{-1}$	$1.24 \times 10^4$
C20	$1.6 \times 10^{-9}$	-2.6	$3.21 \times 10^{-1}$	$2.57 \times 10^4$
C30	$3.4 \times 10^{-9}$	3.8	$5.62 \times 10^{-1}$	$2.04 \times 10^5$
C40	$8.5 \times 10^{-9}$	2.2	$2.07 \times 10^{-1}$	$2.16 \times 10^4$

Figure 5a shows the mobility values of A0, B0, C0, A30, B30, and C30 at various strain values. These results prove that devices with Jeffamine D2000 (B0, B30) and polyurethane (C0, C30) as additives can be stretched to 20% and 50%, respectively. Figure 5b shows the mobility of A0, B0, C0, A30, B30, and C30 at various stretch cycles, indicating that the devices with Jeffamine D2000 (B0, B30) and polyurethane (C0, C30) as additives can be stretched up to 150. The aforementioned results show that the devices with polyurethane additive can achieve superior stretching properties of 50% for stretching 150 cycles. The mobility has almost no change, which is because the polyurethane additive is a softer chain polymer. AFM analysis revealed that the hybrid films with polyurethane always exhibit a denser and more concentrated film structure that is advantageous for the stretching properties of the stretchable devices. In addition, the devices with Jeffamine D2000 can also achieve a good stretching properties of 50% for stretching 150 cycles. Although the mobility is reduced by approximately 10%. However, the A0 and A30 samples without added any additives have a significant problem in that the mobility decreases sharply and does not have stretchability.

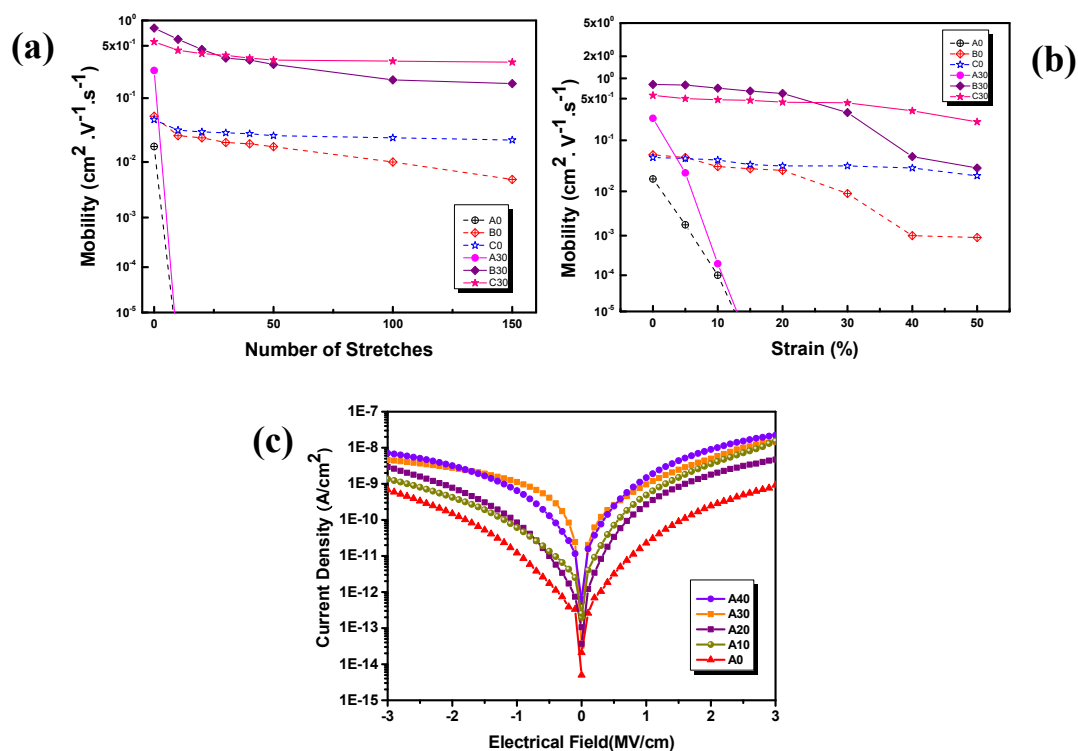


**Figure 5.** (a) mobility of the strained percentage, (b) the strained cycles and (c) leakage characteristics of hybrid thin films.

Finally, we applied three series of dielectric materials (A, B, C) in the OTFT device as gate materials. Table 3 summarizes the electrical characteristics of these OTFTs, including the LCD, mobility, and  $I_{\text{on}}-I_{\text{off}}$ . As mentioned, the electrical properties of the fabricated OTFT devices are identical to those obtained using AFM and surface energy. In the upstretched case, the LCD becomes larger with the increase in the content of  $\text{TiO}_2\text{-SiO}_2$  inorganic nanoparticles, but the LCD value is less than  $10^{-8} \text{ A}\cdot\text{cm}^{-2}$  ( $-2 \text{ MV}\cdot\text{cm}^{-1}$ ) (Figure 5c). The addition of Jeffamine D2000 and polyurethane additives reduces the LCD values. The mobility and  $I_{\text{on}}-I_{\text{off}}$  of the dielectric layers of pure polyimide without inorganic nanoparticles and polymer additives (A0, B0, and C0) are  $1.81 \times 10^{-2} \text{ cm}^2\cdot\text{V}^{-1}\cdot\text{s}^{-1}$  and  $1.13 \times 10^3$  for A0,  $5.04 \times 10^{-2} \text{ cm}^2\cdot\text{V}^{-1}\cdot\text{s}^{-1}$  and  $1.51 \times 10^4$  for B0, and  $4.81 \times 10^{-2} \text{ cm}^2\cdot\text{V}^{-1}\cdot\text{s}^{-1}$  and  $8.13 \times 10^3$  for C0, respectively. The mobility and  $I_{\text{on}}-I_{\text{off}}$  increase obviously with the content of  $\text{TiO}_2\text{-SiO}_2$  inorganic nanoparticles. The mobility and  $I_{\text{on}}-I_{\text{off}}$  of A30 hybrid film reach  $2.42 \times 10^{-1} \text{ cm}^2\cdot\text{V}^{-1}\cdot\text{s}^{-1}$  and  $9.04 \times 10^3$ , respectively. Moreover, after the addition of Jeffamine D2000 (B30) and polyurethane (C30), the mobility and  $I_{\text{on}}-I_{\text{off}}$  improve to  $8.17 \times 10^{-1} \text{ cm}^2\cdot\text{V}^{-1}\cdot\text{s}^{-1}$  and  $4.27 \times 10^5$ , respectively, for B30 and to  $5.62 \times 10^{-1} \text{ cm}^2\cdot\text{V}^{-1}\cdot\text{s}^{-1}$  and  $2.04 \times 10^5$ , respectively, for C30. However, when the content of  $\text{SiO}_2\text{-TiO}_2$  increases to 40 wt.% (A40, B40, and C40), the mobility and switching current ratio decrease to  $1.07 \times 10^{-2} \text{ cm}^2\cdot\text{V}^{-1}\cdot\text{s}^{-1}$  and  $1.16 \times 10^3$ , respectively, for A40 and to  $5.51 \times 10^{-1} \text{ cm}^2\cdot\text{V}^{-1}\cdot\text{s}^{-1}$ , and  $8.50 \times 10^4$ , respectively, for B40, and to  $2.07 \times 10^{-1} \text{ cm}^2\cdot\text{V}^{-1}\cdot\text{s}^{-1}$  and  $2.16 \times 10^3$ , respectively, for C40.

The decreases in mobility and switching current ratio are attributed to the phase separation of the mixed solution when the content of inorganic particles of  $\text{TiO}_2\text{-SiO}_2$  is too high. The results show that the use of  $\text{TiO}_2\text{-SiO}_2$  inorganic nanoparticles and Jeffamine D2000 and polyurethane additives can improve the mobility and  $I_{\text{on}}-I_{\text{off}}$ . However, when the content of  $\text{TiO}_2\text{-SiO}_2$  inorganic nanoparticles reaches 40 wt.%, precipitation and subsequent phase separation occurs in the precursor solution, resulting in poor film properties and thus poor electrical properties for A40, B40, and C40 samples. Therefore, the optimal mass ratio of polyimide and  $\text{TiO}_2\text{-SiO}_2$  inorganic nanoparticles is 70:30 wt.%. The aforementioned results demonstrate that the content of  $\text{TiO}_2\text{-SiO}_2$  nanoparticles exert an obvious influence on the electrical performance of OTFTs. In summary, the mobility and current-switching ratio



of B30- and C30-based OTFT after being stretched 150 cycles at 50% of strain are  $0.29 \text{ cm}^2 \cdot \text{V}^{-1} \cdot \text{s}^{-1}$  and  $8.17 \times 10^4$  for B30-based OTFT and  $0.38 \text{ cm}^2 \cdot \text{V}^{-1} \cdot \text{s}^{-1}$  and  $1.34 \times 10^5$  for C30-based OTFT, respectively, which is higher than those obtained from other hybrid dielectrics-based devices. These results show that Jeffamine D2000 additives (B30) and polyurethane additives (C30) improve the properties of stretchable OTFE devices, of which C30 exerts the better effect. This result is consistent with the optical microscopy result of the tensile test for the hybrid dielectric films.

#### 4. Conclusion

In this study, we successfully synthesized a series of hybrid dielectric films using polyimide and  $\text{SiO}_2$ - $\text{TiO}_2$  nanoparticles without polymer additives, namely polyimide- $\text{TiO}_2$ - $\text{SiO}_2$ , polyimide- $\text{TiO}_2$ - $\text{SiO}_2$ :D2000, and polyimide- $\text{TiO}_2$ - $\text{SiO}_2$ :PU. Pffbt4t-2OD was used in the semiconductor layer. The addition of Jeffamine D2000 (D2000) and polyurethane (PU) as additives was observed to increase the tensile properties without affecting the original electrical properties. The results suggest that the C30-based OTFT achieves the best tensile effect of 50% strain after 150 cycles subject to the 10% mobility reduction because the polyurethane polymers are softer and can provide a denser and more concentrated film structure, which facilitates the stretching of the device. Through the adjustment of the ratios of various  $\text{TiO}_2$ - $\text{SiO}_2$  inorganic nanoparticles, the dielectric constant of the hybrid material can be adjusted, thereby significantly improving the dielectric properties of the dielectric layer. The device properties (mobility and threshold voltage) and film properties (dielectric constant, surface morphology, and hydrophilic hydrophobicity) exhibit a strong correlation to the proportion of  $\text{TiO}_2$ - $\text{SiO}_2$  inorganic nanoparticles. This study shows that the prepared hybrid films can be customized according to the requirements for practical applications. In addition, our PI-hybrid material has the advantage of transparency, high thermal stability, and environmental safety. The addition of Jeffamine D2000 and polyurethane can increase tensile properties without affecting the original electrical properties and widen the applicability of OTFT devices.

**Supplementary Materials:** The following are available online at <http://www.mdpi.com/2073-4360/12/5/1058/s1>, Figure S1: The TEM image of inorganic  $\text{TiO}_2$ - $\text{SiO}_2$  nanoparticles; Figure S2: The optical transmittance of A0, A30, B30, and C30 films as the dielectric layer of OTFTs device; Figure S3: The transfer curves of OTFTs prepared by different dielectric layer materials, A0, A30, B30, and C30; Figure S4: The output characteristics of the OTFTs prepared by different dielectric layer materials: (a) A0, (b) A30, (c) B30, and (d) C30.

**Author Contributions:** Conceptualization, Y.-Y.Y.; Data curation, C.-H.Y.; Funding acquisition, Y.-Y.Y.; Investigation, Y.-Y.Y. and C.-H.Y.; Methodology, C.-H.Y.; Project administration, Y.-Y.Y.; Supervision, Y.-Y.Y.; Writing—original draft, Y.-Y.Y.; Writing—review & editing, Y.-Y.Y. All authors have read and agreed to the published version of the manuscript.

**Acknowledgments:** We thank the Ministry of Science and Technology of Taiwan (MOST 108-2221-E-131-003) for providing financial support.

**Conflicts of Interest:** The authors declare no conflict of interest.

#### References

1. Qian, Y.; Zhang, X.W.; Xie, L.H.; Qi, D.P.; Chandran, B.K.; Chen, X.D.; Huang, W. Stretchable Organic Semiconductor Devices. *Adv. Mater.* **2016**, *28*, 9243–9265. [[CrossRef](#)] [[PubMed](#)]
2. Forrest, S.R. The path to ubiquitous and low-cost organic electronic appliances on plastic. *Nature* **2004**, *428*, 911–918. [[CrossRef](#)] [[PubMed](#)]
3. Hsieh, Y.T.; Chen, J.Y.; Fukuta, S.; Lin, P.C.; Higashihara, T.; Chueh, C.C.; Chen, W.C. Realization of Intrinsically Stretchable Organic Solar Cells Enabled by Charge-Extraction Layer and Photoactive Material Engineering. *ACS Appl. Mater. Interfaces* **2018**, *10*, 21712–21720. [[CrossRef](#)]
4. Shekar, B.C.; Lee, J.Y.; Rhee, S.W. Organic thin film transistors: Materials, process and devices. *Korean J. Chem. Eng.* **2004**, *21*, 267–285. [[CrossRef](#)]
5. Kumar, B.; Kaushik, B.K.; Negi, Y.S. Organic Thin Film Transistors: Structures, Models, Materials, Fabrication, and Applications: A Review. *Polym. Rev.* **2014**, *54*, 33–111. [[CrossRef](#)]



6. Golmar, F.; Gobbi, M.; Llopis, R.; Stoliar, P.; Casanova, F.; Hueso, L.E. Non-conventional metallic electrodes for organic field-effect transistors. *Org. Electron.* **2012**, *13*, 2301–2306. [[CrossRef](#)]
7. Wen, H.F.; Wu, H.C.; Aimi, J.; Hung, C.C.; Chiang, Y.C.; Kuo, C.C.; Chen, W.C. Soft Poly(butyl acrylate) Side Chains toward Intrinsically Stretchable Polymeric Semiconductors for Field-Effect Transistor Applications. *Macromolecules* **2017**, *50*, 4982–4992. [[CrossRef](#)]
8. Wang, J.T.; Takshima, S.; Wu, H.C.; Shih, C.C.; Isono, T.; Kakuchi, T.; Satoh, T.; Chen, W.C. Stretchable Conjugated Rod Coil Poly(3-hexylthiophene)-block-poly(butyl acrylate) Thin Films for Field Effect Transistor Applications. *Macromolecules* **2017**, *50*, 1442–1452. [[CrossRef](#)]
9. Lee, W.Y.; Wu, H.C.; Lu, C.; Naab, B.D.; Chen, W.C.; Bao, Z.N. n-Type Doped Conjugated Polymer for Nonvolatile Memory. *Adv. Mater.* **2017**, *29*. [[CrossRef](#)]
10. Oh, J.Y.; Rondeau-Gagne, S.; Chiu, Y.C.; Chortos, A.; Lissel, F.; Wang, G.J.N.; Schroeder, B.C.; Kurosawa, T.; Lopez, J.; Katsumata, T.; et al. Intrinsically stretchable and healable semiconducting polymer for organic transistors. *Nature* **2016**, *539*, 411–415. [[CrossRef](#)]
11. Kumar, B.; Kaushik, B.K.; Negi, Y.S. Perspectives and challenges for organic thin film transistors: Materials, devices, processes and applications. *J. Mater. Sci. Mater. Electron.* **2014**, *25*, 1–30. [[CrossRef](#)]
12. Wang, B.H.; Huang, W.; Chi, L.F.; Al-Hashimi, M.; Marks, T.J.; Facchetti, A. High-k Gate Dielectrics for Emerging Flexible and Stretchable Electronics. *Chem. Rev.* **2018**, *118*, 5690–5754. [[CrossRef](#)] [[PubMed](#)]
13. Han, G.Q.; Wang, X.M.; Zhang, J.; Zhang, G.C.; Yang, H.H.; Hu, D.B.; Sun, D.W.; Wu, X.M.; Ye, Y.; Chen, H.P.; et al. Interface engineering with double-network dielectric structure for flexible organic thin film transistors. *Org. Electron.* **2018**, *52*, 213–221. [[CrossRef](#)]
14. Hung, C.C.; Wu, H.C.; Chiu, Y.C.; Tung, S.H.; Chen, W.C. Crosslinkable high dielectric constant polymer dielectrics for low voltage organic field-effect transistor memory devices. *J. Polym. Sci. Part A Polym. Chem.* **2016**, *54*, 3224–3236. [[CrossRef](#)]
15. McCoul, D.; Hu, W.L.; Gao, M.M.; Mehta, V.; Pei, Q.B. Recent Advances in Stretchable and Transparent Electronic Materials. *Adv. Electron. Mater.* **2016**, *2*. [[CrossRef](#)]
16. Han, D.D.; Chen, Z.F.; Cong, Y.Y.; Yu, W.; Zhang, X.; Wang, Y. High-Performance Flexible Tin-Zinc-Oxide Thin-Film Transistors Fabricated on Plastic Substrates. *IEEE Trans. Electron Devices* **2016**, *63*, 3360–3363. [[CrossRef](#)]
17. Sekine, T.; Fukuda, K.; Kumaki, D.; Tokito, S. Highly stable flexible printed organic thin-film transistor devices under high strain conditions using semiconducting polymers. *Jpn. J. Appl. Phys.* **2015**, *54*. [[CrossRef](#)]
18. Lim, J.W.; Koo, J.B.; Yun, S.J.; Kim, H.T. Characteristics of pentacene thin film transistor with Al<sub>2</sub>O<sub>3</sub> gate dielectrics on plastic substrate. *Electrochem. Solid-State Lett.* **2007**, *10*, J136–J138. [[CrossRef](#)]
19. Shih, C.C.; Lee, W.Y.; Lu, C.; Wu, H.C.; Chen, W.C. Enhancing the Mechanical Durability of an Organic Field Effect Transistor through a Fluoroelastomer Substrate with a Crosslinking-Induced Self-Wrinkled Structure. *Adv. Electron. Mater.* **2017**, *3*. [[CrossRef](#)]
20. Song, L.; Wang, Y.; Gao, Q.; Guo, Y.; Wang, Q.J.; Qian, J.; Jiang, S.; Wu, B.; Wang, X.R.; Shi, Y.; et al. Speed up Ferroelectric Organic Transistor Memories by Using Two-Dimensional Molecular Crystalline Semiconductors. *ACS Appl. Mater. Interfaces* **2017**, *9*, 18127–18133. [[CrossRef](#)]
21. Hsu, H.H.; Chang, C.Y.; Cheng, C.H. Room-temperature flexible thin film transistor with high mobility. *Curr. Appl. Phys.* **2013**, *13*, 1459–1462. [[CrossRef](#)]
22. Yu, Y.Y.; Liu, C.L.; Chen, Y.C.; Chiu, Y.C.; Chen, W.C. Tunable dielectric constant of polyimide-barium titanate nanocomposite materials as the gate dielectrics for organic thin film transistor applications. *RSC Adv.* **2014**, *4*, 62132–62139. [[CrossRef](#)]
23. Zhang, C.Y.; Wang, H.; Shi, Z.S.; Cui, Z.C.; Yan, D.H. UV-directly patternable organic-inorganic hybrid composite dielectrics for organic thin-film transistors. *Org. Electron.* **2012**, *13*, 3302–3309. [[CrossRef](#)]
24. Lee, W.H.; Wang, C.C.; Ho, J.C. Influence of nano-composite gate dielectrics on OTFT characteristics. *Thin Solid Films* **2009**, *517*, 5305–5310. [[CrossRef](#)]
25. Jung, S.W.; Koo, J.B.; Park, C.W.; Na, B.S.; Park, N.M.; Oh, J.Y.; Moon, Y.G.; Lee, S.S.; Koo, K.W. Non-volatile organic ferroelectric memory transistors fabricated using rigid polyimide islands on an elastomer substrate. *J. Mater. Chem. C* **2016**, *4*, 4485–4490. [[CrossRef](#)]
26. Damaceanu, M.D.; Constantin, C.P.; Bruma, M.; Belomoina, N.M. Highly fluorinated polyimide blends—Insights into physico-chemical characterization. *Polymer* **2014**, *55*, 4488–4497. [[CrossRef](#)]

27. Ahn, T.; Kim, J.W.; Choi, Y.; Yi, M.H. Hybridization of a low-temperature processable polyimide gate insulator for high performance pentacene thin-film transistors. *Org. Electron.* **2008**, *9*, 711–720. [[CrossRef](#)]
28. Kim, Y.J.; Kim, J.; Kim, Y.S.; Lee, J.K. TiO<sub>2</sub>-poly(4-vinylphenol) nanocomposite dielectrics for organic thin film transistors. *Org. Electron.* **2013**, *14*, 3406–3414. [[CrossRef](#)]
29. Chu, C.W.; Li, S.H.; Chen, C.W.; Shrotriya, V.; Yang, Y. High-performance organic thin-film transistors with metal oxide/metal bilayer electrode. *Appl. Phys. Lett.* **2005**, *87*. [[CrossRef](#)]
30. Tsai, C.L.; Chen, C.J.; Wang, P.H.; Lin, J.J.; Liou, G.S. Novel solution-processable fluorene-based polyimide/TiO<sub>2</sub> hybrids with tunable memory properties. *Polym. Chem.* **2013**, *4*, 4570–4573. [[CrossRef](#)]
31. Zhao, J.B.; Li, Y.K.; Yang, G.F.; Jiang, K.; Lin, H.R.; Ade, H.; Ma, W.; Yan, H. Efficient organic solar cells processed from hydrocarbon solvents. *Nat. Energy* **2016**, *1*. [[CrossRef](#)]
32. Scenev, V.; Cosseddu, P.; Bonfiglio, A.; Salzmann, I.; Severin, N.; Oehzelt, M.; Koch, N.; Rabe, J.P. Origin of mechanical strain sensitivity of pentacene thin-film transistors. *Org. Electron.* **2013**, *14*, 1323–1329. [[CrossRef](#)]
33. Tsai, M.H.; Huang, Y.C.; Tseng, I.H.; Yu, H.P.; Lin, Y.K.; Huang, S.L. Thermal and mechanical properties of polyimide/nano-silica hybrid films. *Thin Solid Films* **2011**, *519*, 5238–5242. [[CrossRef](#)]
34. Chou, W.Y.; Ho, T.Y.; Cheng, H.L.; Tang, F.C.; Chen, J.H.; Wang, Y.W. Gate field induced ordered electric dipoles in a polymer dielectric for low-voltage operating organic thin-film transistors. *RSC Adv.* **2013**, *3*, 20267–20272. [[CrossRef](#)]
35. Huang, T.S.; Su, Y.K.; Wang, P.C. Study of organic thin film transistor with polymethylmethacrylate as a dielectric layer. *Appl. Phys. Lett.* **2007**, *91*. [[CrossRef](#)]
36. Miskiewicz, P.; Kotarba, S.; Jung, J.; Marszalek, T.; Mas-Torrent, M.; Gomar-Nadal, E.; Amabilino, D.B.; Rovira, C.; Veciana, J.; Maniukiewicz, W.; et al. Influence of SiO<sub>2</sub> surface energy on the performance of organic field effect transistors based on highly oriented, zone-cast layers of a tetrathiafulvalene derivative. *J. Appl. Phys.* **2008**, *104*. [[CrossRef](#)]
37. Savagatrup, S.; Chan, E.; Renteria-Garcia, S.M.; Printz, A.D.; Zaretski, A.V.; O'Connor, T.F.; Rodriguez, D.; Valle, E.; Lipomi, D.J. Plasticization of PEDOT:PSS by Common Additives for Mechanically Robust Organic Solar Cells and Wearable Sensors. *Adv. Funct. Mater.* **2015**, *25*, 427–436. [[CrossRef](#)]
38. Lu, C.; Lee, W.Y.; Shih, C.C.; Wen, M.Y.; Chen, W.C. Stretchable Polymer Dielectrics for Low-Voltage-Driven Field-Effect Transistors. *ACS Appl. Mater. Interfaces* **2017**, *9*, 25522–25532. [[CrossRef](#)] [[PubMed](#)]
39. Wang, C.; Lee, W.Y.; Nakajima, R.; Mei, J.G.; Kim, D.H.; Bao, Z.A. Thiol-ene Cross-Linked Polymer Gate Dielectrics for Low-Voltage Organic Thin-Film Transistors. *Chem. Mater.* **2013**, *25*, 4806–4812. [[CrossRef](#)]
40. Jiang, B.H.; Peng, Y.J.; Chen, C.P. Simple structured polyetheramines, Jeffamines, as efficient cathode interfacial layers for organic photovoltaics providing power conversion efficiencies up to 9.1%. *J. Mater. Chem. A* **2017**, *5*, 10424–10429. [[CrossRef](#)]
41. Huang, Z.Q.; Hu, X.T.; Liu, C.; Tan, L.C.; Chen, Y.W. Nucleation and Crystallization Control via Polyurethane to Enhance the Bendability of Perovskite Solar Cells with Excellent Device Performance. *Adv. Funct. Mater.* **2017**, *27*. [[CrossRef](#)]
42. Yu, Y.Y.; Huang, T.J.; Lee, W.Y.; Chen, Y.C.; Kuo, C.C. Highly transparent polyimide/nanocrystalline-zirconium dioxide hybrid materials for organic thin film transistor applications. *Org. Electron.* **2017**, *48*, 19–28. [[CrossRef](#)]
43. Yu, Y.Y.; Chiu, C.T.; Chueh, C.C. Solution-Processable, Transparent Polyimide for High-Performance High-k Nanocomposite: Synthesis, Characterization, and Dielectric Applications in Transistors. *Asian J. Org. Chem.* **2018**, *7*, 2263–2270. [[CrossRef](#)]
44. Yang, B.X.; Tseng, C.Y.; Chiang, A.S.T.; Liu, C.L. A sol-gel titanium-silicon oxide/organic hybrid dielectric for low-voltage organic thin film transistors. *J. Mater. Chem. C* **2015**, *3*, 968–972. [[CrossRef](#)]
45. Baeg, K.J.; Noh, Y.Y.; Sirringhaus, H.; Kim, D.Y. Controllable Shifts in Threshold Voltage of Top-Gate Polymer Field-Effect Transistors for Applications in Organic Nano Floating Gate Memory. *Adv. Funct. Mater.* **2010**, *20*, 224–230. [[CrossRef](#)]
46. Naber, R.C.G.; Tanase, C.; Blom, P.W.M.; Gelinck, G.H.; Marsman, A.W.; Touwslager, F.J.; Setayesh, S.; De Leeuw, D.M. High-performance solution-processed polymer ferroelectric field-effect transistors. *Nat. Mater.* **2005**, *4*, 243–248. [[CrossRef](#)]

